Kinetics and Catalysis, Vol. 42, No. 3, 2001, pp. 354–365. Translated from Kinetika i Kataliz, Vol. 42, No. 3, 2001, pp. 394–405.
Original Russian Text Copyright © 2001 by Ivanova.

IV RUSSIAN CONFERENCE WITH THE PARTICIPATION OF CIS COUNTRIES ON THE SCIENTIFIC BASES OF CATALYST PREPARATION AND TECHNOLOGY

Highly Dispersed Zirconium-Containing Oxide Systems: Synthesis, Properties, and Applications

A. S. Ivanova

Boreskov Institute of Catalysis, Siberian Division, Russian Academy of Sciences, Novosibirsk, 630090 Russia

Received September 18, 2000

Abstract—The formation of the phase composition, dispersion, pore structure, and surface state of binary zirconium-containing systems was examined depending on the nature and concentration of the second component, preparation conditions and procedures, and thermal treatment conditions. Various types of interactions were found, which are governed by the nature of the second component and the treatment temperature. The effects of surfactants on the physicochemical properties of precipitates depend on the conditions of synthesis: the surfactant amount retained by a precipitate at pH 3–4 is greater than that at pH 9 by an order of magnitude. The thermolysis of samples synthesized at acidic pH, along with dehydration and dehydroxylation, is accompanied by the decomposition and degradation of surfactants. Because of this, certain compounds and their fragments capable of reducing corresponding phases are removed stepwise. Highly dispersed compositions were obtained at 110–400°C with a minimum particle size of 2.5–16 nm; at 700°C, the particle size was no higher than 20 nm. The ratio between the ionic radii of added and main components is a factor determining the dispersion of formed phases. In this case, changes in the nature of surfactants and in the conditions of a particular synthesis make it possible to prepare highly dispersed systems with monomesoporous structures. The total volume and the average diameter of pores can be controlled over wide limits.

INTRODUCTION

Zirconium-containing oxide systems are widely used in catalysis, ceramics, and refractories industry and as solid electrolytes. According to Burch [1], zirconium-containing catalysts are used in the dehydration, isomerization, alkylation, selective oxidation, and full oxidation of hydrocarbons; polymerization; oxychlorination; steam reforming; Fischer–Tropsch synthesis; etc.

This widespread use of zirconium-containing oxide systems results from the diversity and structure peculiarities of ZrO_2 modifications. Individual ZrO_2 occurs as the following modifications [2]: amorphous, low-temperature tetragonal, low-temperature cubic, monoclinic, high-temperature tetragonal, and high-temperature cubic. The first three modifications are metastable phases, and they are readily converted into monoclinic ZrO_2, which is characterized by a stable structure and a low specific surface area. Thus, in particular, hydroxide samples calcined at 700°C consisted of monoclinic ZrO_2, whose specific surface area varied within the range 10–30 m^2/g [3]. Therefore, various studies of zirconium-containing systems are primarily oriented to (1) the stabilization of low-temperature ZrO_2 modifications (cubic and tetragonal) and (2) the possibility of preparing ZrO_2-based compounds with the perovskite ($M(II)ZrO_3$) and pyrochlore ($(M(III))_2Zr_2O_7$) structures.

According to published data [4–10], the low-temperature cubic ZrO_2 modification, which is characterized by higher dispersion compared with the monoclinic modification, is stabilized by the addition of either cations (Mg^{2+}, Ca^{2+}, Y^{3+}, Sc^{3+}, etc.) or anions (SO_4^{2-}, and PO_4^{3-}). In particular, many studies (see, for example, the reviews [9, 10]) were devoted to the physicochemical and catalytic properties of sulfated ZrO_2, which exhibits unique acid properties. Thus, most attention was focused on the stabilization of ZrO_2 with various cations. In this case, the statement by Naumov *et al.* [11] that the stability of cubic ZrO_2 is possible only in the presence of the anionic vacancies ZrO_{2-x} was taken into consideration.

Note that interest in the production and use of highly dispersed systems and nanocrystalline materials, among them ZrO_2-based materials, has quickened in the past few years. A procedure for controlling the dispersion of binary oxide systems may consist in changing the ratio between the ionic radii of added and main cations [12]. Another feasible procedure for changing the particle size of hydroxide and oxide systems can be the sol–gel synthesis, which makes it possible to vary broadly precipitation conditions [13, 14].

A cyclic tetramer is the main Zr(IV) species in an aqueous solution; it undergoes hydrolysis according to the reaction [15]

$$[Zr_4(OH)_8(H_2O)_{16}]^{8+} + 4H_2O \longrightarrow$$

$$\longrightarrow [Zr_4(OH)_{12}(H_2O)_{12}]^{4+} + H_3O^+.$$

Polynuclear hydroxo complexes and colloid particles of a hydroxide phase are formed as a result of this pro-

0023-1584/01/4203-0354$25.00 © 2001 MAIK “Nauka / Interperiodica”

cess. Thus, Baes and Mesmer [16] noted that stepwise complexation and the formation of complexes of the composition $[Zr(OH)_n]^{4-n}$ takes place at low Zr(IV) concentrations. More recently [17], the following regions of preference were determined for complexes of specific compositions:

$$0 \le pH \le 2.0\ [Zr(OH)]^{3+},\quad 4.6 \le pH \le 6.3\ Zr(OH)_4;$$

$$2.0 \le pH \le 3.4\ [Zr(OH)_2]^{2+},\quad 6.3 \le pH \le 8.1\ [Zr(OH)_5]^{-};$$

$$3.4 \le pH \le 4.6\ [Zr(OH)_3]^{+},\quad 8.1 \le pH\ [Zr(OH)_6]^{2-}.$$

Consequently, the properties of precipitates, in particular, the particle size, depend on pH at which the precipitation of components was completed.

The dispersion of oxide systems synthesized by the sol–gel method can also be controlled by the addition of surfactants [18]. This is possible because, as a rule, the presence of surfactants decreases the surface tension of an intermicellar liquid and affects the size, morphology, and the spatial orientation of resulting crystals.

On this basis, the binary oxide systems M–Zr–O (M = Ca, Sr, Ba, Y, Fe, La, Sm, Yb, and Ce) differring in their preparation conditions and procedures, as well as in the nature of present surfactants, were chosen as test materials.

The limits of pH at which the system components can be coprecipitated should be determined before the synthesis of the M–Zr–O systems. For example, in accordance with the titration curves of 0.5 mol/l solutions of zirconyl, calcium, iron, and samarium nitrates, which were given in [19], the precipitation of iron and zirconium hydroxides begins at somewhat different pH values of 1.5 and 2.0, respectively. The precipitation of zirconium, samarium, and calcium hydroxides begins at considerably different pH values (2.0, 7.0, and 11.5, respectively). Consequently, the degree of sample homogeneity can be lower in this case. On the other hand, analysis of the titration curves provides an opportunity to choose a pH value at which the maximum completeness of precipitation and the homogeneity of synthesized precipitates are achieved.

Formation of zirconium-containing oxide systems prepared by precipitation at constant pH. It was found [13, 20–28] that the introduction of ≤25 mol % M_nO_m into ZrO_2 followed by thermal treatment at 400–1000°C causes a loss of oxygen as a result of the isomorphous replacement of Zr^{4+} with $M^{2+(3+)}$. The coordination numbers of introduced cations are changed, and the highly symmetrical and highly dispersed solid solutions $(Zr_{1-x}M_x^{2+})O_{2-x}$ and $(Zr_{1-x}M_x^{3+})O_{2-x/2}$ are formed on the basis of cubic zirconium dioxide. Taking into account the structure peculiarities of fluorite (cubic ZrO_2 crystallizes as this structure), in the treatment of these structures, it is common practice to consider a disordered distribution of polyhedrons typical of particular cations because of an irregularity of oxygen vacancies rather than a disorder in the population of cations. It is believed that the statistically disordered distribution of polyhedrons in the structure stabilizes ZrO_2 in a more symmetrical strained form. The unit-cell parameters of the above solid solution depend on the nature and concentration of introduced components and, to a smaller extent, on the treatment temperature.

In the M–Zr–O (M = Ca, Sr, and Ba) systems, the above parameters could not be determined for the majority of compositions because a mixture of tetragonal and monoclinic ZrO_2 is formed at the concentration [MO] ≤ 10 mol % and a mixture of cubic and monoclinic ZrO_2 is formed at 10 < [MO] ≤ 25 mol %. Consequently, the determination of the *a* parameter would be incorrect because of the overlapping peaks of the above phases in X-ray diffraction patterns. In the M–Zr–O (M = Y, La, Sm, and Yb) systems, the unit-cell parameter of a solid solution obtained at 700°C increases from 5.144 to 5.190 Å in the order Y ⟶ Sm ⟶ La in accordance with the ionic radii.

After the introduction of ~33–35 mol % M_nO_m into ZrO_2, new phases are formed in addition to the above solid solution based on cubic ZrO_2: excessive M_nO_m, a solid solution on its basis, or a compound with the pyrochlore structure. This is illustrated by the following reaction scheme:

$$\text{Yb–Zr–O} \xrightarrow{350\text{–}1000^\circ\text{C}} (Zr_{1-x}Yb_x)O_{2-x/2},\quad r_{Yb}^{3+} = 1.00\ \text{Å};$$

$$\text{Y–Zr–O} \xrightarrow{700\text{–}900^\circ\text{C}} (Zr_{1-x}Y_x)O_{2-x/2} + Y_2O_3,$$

$$r_Y^{3+} = 1.06\ \text{Å};$$

$$\text{Sm–Zr–O} \xrightarrow{350\text{–}1000^\circ\text{C}} (Zr_{1-x}Sm_x)O_{2-x/2} + (Sm,Zr)_2O_3,$$

$$r_{Sm}^{3+} = 1.13\ \text{Å};$$

$$\text{La–Zr–O} \xrightarrow{700^\circ\text{C}} \text{Amorphous phase} \xrightarrow{800\text{–}1000^\circ\text{C}} La_2Zr_2O_7,$$

$$r_{La}^{3+} = 1.22\ \text{Å}.$$

The following two factors are responsible for the presence of a second phase in a number of samples: the restricted solubility of the added component in a ZrO_2 matrix (the amount of an excessive phase increases with the ionic radius of the introduced cation) and the incompleteness of reaction between components (this reaction can be enhanced by increasing the treatment temperature) [29, 30]. A compound with the pyrochlore structure is formed only in the La–Zr–O system. This is due to the fulfillment of the condition $r_{La}^{3+}/r_{Zr}^{4+} > 1.2$, which is necessary for the stability of the pyrochlore structure [31].

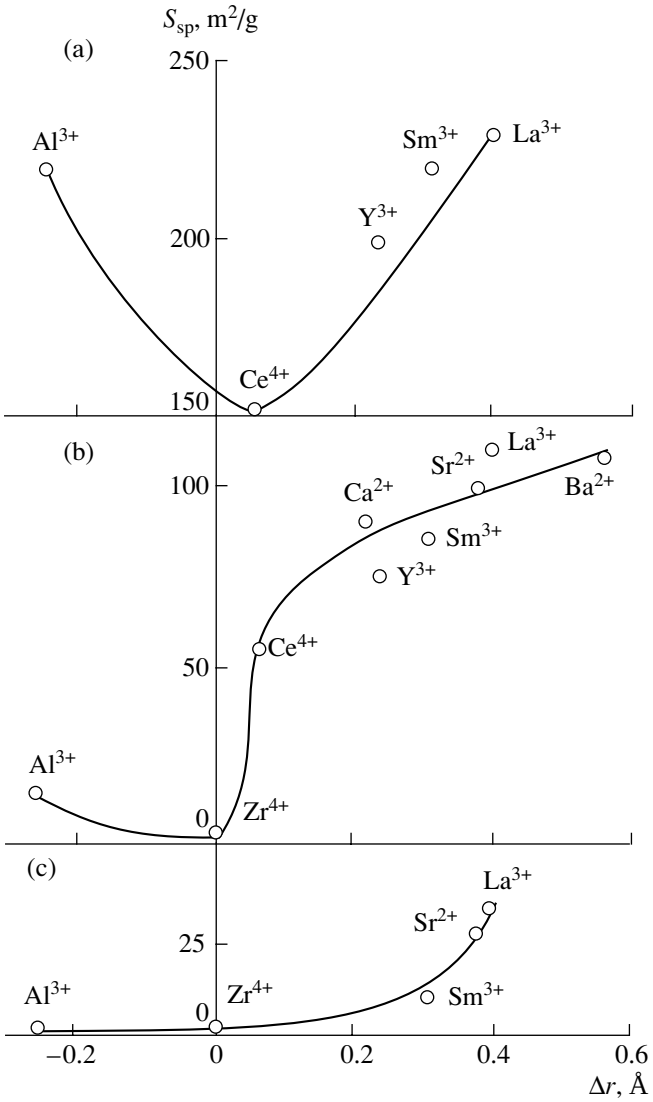

Fig. 1. Specific surface areas of M–Zr–O samples containing 10 mol % M_nO_m calcined at (a) 400, (b) 700, and (c) 1000°C as functions of the difference between the ionic radii of added (M) and base (Zr) components.

After the introduction of ~50 mol % M_nO_m into ZrO_2, the phase composition in M_2O_3–ZrO_2 remains almost the same as that at $[M_nO_m] \approx 33$ mol %; a La_2O_3 phase appears only in the La–Zr–O system. Perovskite is formed in the MO–ZrO_2 systems [32]. This formation consists in the ordering of a metastable phase based on cubic ZrO_2 with the ratio $M^{2+}/Zr^{4+} \sim 1$ in the range 350–800°C followed by its transformation and decomposition to $(Zr_{1-x}M_x^{2+})O_{2-x}$ and $M^{2+}ZrO_3$ at 805–810°C:

$$\text{Ca–Zr–O} \xrightarrow{550^\circ\text{C}} (\text{Zr,Ca})\text{O}_2$$

$$\xrightarrow{800\text{–}1000^\circ\text{C}} (\text{Zr}_{1-x}\text{Ca}_x)\text{O}_{2-x} + \text{CaZrO}_3.$$

The Ce–Zr–O system holds a particular position: because the ionic radii of cerium and zirconium are similar and the oxide structures are isomorphous over a wide concentration range, a mixture of solid solutions based on cubic zirconium and cerium dioxides is formed [13], namely:

$$\text{CeO}_2(10\text{–}90\text{ mol \%}) + \text{ZrO}_2$$

$$\xrightarrow{400\text{–}1000^\circ\text{C}} (\text{Zr}_{1-x}\text{Ce}_x)\text{O}_2 + (\text{Ce}_{1-x}\text{Zr}_x)\text{O}_2.$$

A special feature of the above zirconium-containing binary systems is their high dispersion because the particle size of the corresponding phases is no higher than 30–50 nm even in the temperature range 700–1000°C, whereas the particle size of individual ZrO_2 is higher by an order of magnitude.

Accordingly, the specific surface areas of binary samples containing 10 mol % M_nO_m and calcined at 400°C was higher than the surface area of pure ZrO_2 in all cases (Fig. 1a). The greater the difference between the ionic radii of added and main components, the higher the surface area of binary samples. That is, the condition observed for aluminum-containing binary systems [12] is also fulfilled for zirconium-containing binary systems. The character of the dependence remained unchanged as the treatment temperature was increased (Figs. 1b and 1c); only the absolute value of the specific surface area decreased.

Formation of zirconium-containing oxide systems prepared by precipitation at variable pH. It is well known [33, 34] that, on the addition of a base to salt solutions, hydrolysis and polycondensation reactions occur to form polynuclear hydroxo complexes, which, in turn, affect the properties of the resulting precipitates. According to Fedotov et al. [33, 35], on the addition of a base to concentrated (≥0.1 mol/l) solutions of Al^{3+}, Fe^{3+}, and Cr^{3+} salts or their mixtures, the above reactions occur by the scheme $M^{3+} \longrightarrow [MOH]^{2+} \longrightarrow [M_2(OH)_2]^{4+} \longrightarrow [M_p(OH)_n]^{3p-n} \longrightarrow M_q \longrightarrow$ precipitate, where M_p is a polynuclear hydroxo complex ($p > 2$) and M_q is a colloid particle (coordinated H_2O molecules are omitted in the above scheme).

The concentration of mononuclear species (M^{3+} + $[MOH]^{2+}$) in solutions with paramagnetic ions (Fe^{3+}, Cr^{3+}) can be evaluated by the ^{2}D NMR line width of water. The contribution to the line width from polynuclear paramagnetic species is small because of a decrease in the effective magnetic moment of ions because of the spin–spin interaction. The formation of colloid particles causes a dramatic line widening in ^{14}N and ^{35}Cl NMR spectra. This fact makes it possible to detect the M_q particles in solution.

It was found in ^{2}D and ^{14}N NMR studies of zirconyl nitrate solutions with the addition of a base [36] that sol particles insignificantly contribute to the line widths of water and NO_3^- in the spectra of the above nuclei. Therefore, a more sensitive indicator of the formation

of colloid particles—chloride ions—was added to the solution. These ions made it possible to reliably determine the value χ([OH]/[Zr]) at which colloid particles appear. They were detected in a solution of individual zirconyl nitrate at $\chi \geq 2.50$ [36], whereas the formation of colloid particles in mixed zirconium-containing solutions depends on the nature and concentration of the other component. Thus, the changes observed in iron–zirconium nitric acid solutions depend on the ratio between the components $\gamma([Fe^{3+}]/[Zr^{4+}])$. It was found that an increase in γ from 0.02 to 0.60 leads to an increase in the rate of hydrolysis and polycondensation, as evidenced by the values of χ, which decreased from 2.20 to 1.38, respectively.

Another behavior was observed in yttrium–zirconium and lanthanum–zirconium solutions on the addition of a base. This is due to the fact that the pH values for the precipitation of added components are much higher than that for zirconium: yttrium and lanthanum are precipitated at pH ≥ 6.95 [37] and pH ≥ 8.35 [38], respectively. Therefore, zirconium and yttrium (lanthanum) ions are hydrolyzed separately, and the formation of colloid particles is observed at high pH values.

The formation of the phase composition in the M–Zr–O binary systems (M = Fe, Y, or La) precipitated at final pH 9 takes place in the same manner [36] as in the samples prepared at constant pH [13, 28]. Over the range 110–400°C, the compositions under consideration are mainly amorphous to X-rays. Only in the Fe–Zr–O samples with $\gamma \approx 0.60$, an α-Fe_2O_3 phase is formed starting from 110°C. It is likely that the crystallization of hematite at this low temperature depends on the temperature of aging (~100°C). Lukachina *et al.* [37] reported on a possible effect of this factor. An increase in the temperature to 700°C facilitates crystallization in all samples of a solid solution based on cubic ZrO_2. Its unit-cell parameters increase on the replacement of the second component in the order Fe ⟶ Y ⟶ La, all other factors being the same; this is also consistent with the ionic radii. Only in the Y–Zr–O samples with $\gamma \approx 0.60$, an Y_2O_3 phase was not detected, which was observed in the samples prepared at constant pH [28]. It is likely that the Y_2O_3 phase is present in a highly dispersed state, which is not detected by X-ray diffraction analysis, or the synthesis procedure in use increases the degree of Y^{3+} incorporation into ZrO_2.

The Fe–Zr–O samples with $\gamma = 0.12$ different in the treatment temperatures were studied by electron microscopy [39]. The structures of these samples were found to be almost identical (Fig. 2): the particles were dense aggregates ~100 nm in size with a disordered polycrystalline structure that consists of chaotically disoriented primary crystallites of sizes no greater than 1–1.5 nm. In this case, crystallite lattice planes with an interplanar spacing of about 0.3 nm, which corresponds to the interplanar spacing d_{111} of the cubic structure of ZrO_2, can be observed. The crystallites exhibit microdistortions, which manifest themselves in warped (111) planes. Thus, it may be concluded that even at 110–400°C the fragments of a cubic ZrO_2 phase occur in the structure of the sample despite of a strong disorder.

Phase transitions are changed on going to compositions prepared at acidic pH. This is reflected in the fact that, first, a solid solution based on cubic ZrO_2 is formed even at 400°C [36] and, second, its unit-cell parameter is greater than that in samples prepared at pH 9. The reason is that the fraction of low-molecular species containing an amount of anions [39, 40] sufficient for the stabilization of a cubic ZrO_2 modification increases in the region of low pH values.

The crystallite size found by X-ray diffraction analysis in samples calcined at 700°C varied within the limits 3.5–16.0 nm for the phase of a solid solution based on cubic ZrO_2 and 20–47 nm for α-Fe_2O_3. The high dispersion of the samples was also supported by adsorption data.

The specific surface areas of binary samples prepared at final pH 9 and dried at 110°C decreased from 500 (±20) to 350, 200, or 150 (±50) m^2/g with an increase in the fraction of the second component in iron–, yttrium–, or lanthanum–zirconia samples, respectively (Fig. 3a). In particular, the surface area of Fe–Zr–O samples prepared at pH ≤ 7 is lower than that for pH 9. This is due to the presence of nitrates [36], in the presence of which the specific surface areas of the majority of hydroxide systems decrease [41].

An increase in the temperature of sample treatment resulted in a decrease in the specific surface area (Figs. 3b and 3c). In this case, the character of the dependence of the specific surface area on the fraction of the second component was retained in the samples synthesized at pH 9. In the Fe–Zr–O samples prepared at pH ≤ 7, the specific surface area increased with γ (Fig. 3b) and reached a value typical of the samples synthesized at pH 9.

Effects of surfactants on the formation of the phase composition, dispersion, and pore structure. These effects were considered using the Fe–Zr–O system with $\gamma = 0.12$ as an example. The solutions of glycerol, polyvinyl alcohol (PVA), carboxymethyl cellulose (CMC), sodium ethylenediaminetetraacetate (EDTA), and sodium stearate were used as surfactants.

It was found [42] that the presence of surfactants inhibits the formation of colloid particles. Depending on the nature of surfactants, the following order was observed:

Surfactant:	0	≤ PVA	< Glycerol	< CMC
χ:	1.77	1.80	2.04	2.27

It is likely that added surfactants participate in the hydrolysis of iron and zirconyl nitrates. This was supported by the fact that glycerol in an aqueous solution was readily detected by ^{13}C NMR signals, whereas it was not detected in iron–zirconium solutions. Taking into account that, according to [15], the hydrolysis of

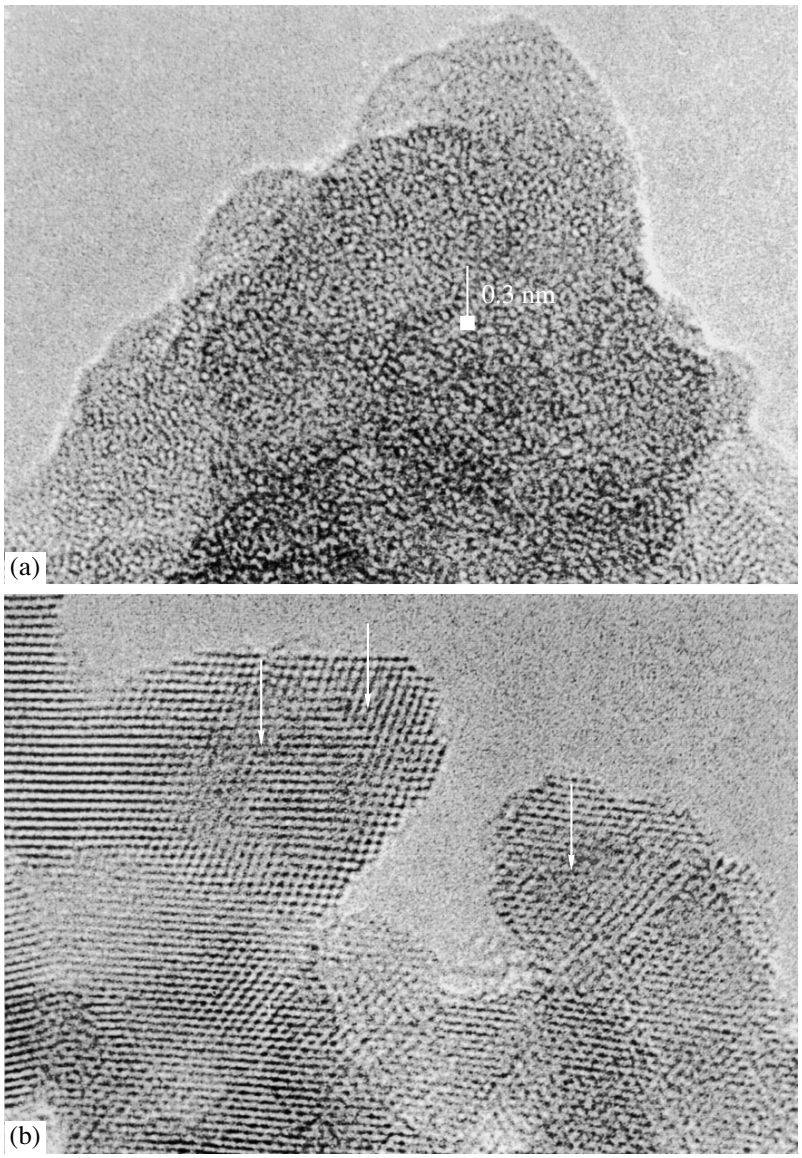

Fig. 2. Electron micrographs of Fe–Zr–O samples calcined at (a) 400 and (b) 700°C. Arrows indicate clusters with disordered structures.

zirconium-containing solutions is accompanied by the release of protons, we may believe that protons are associated with the added surfactants to inhibit the hydrolysis.

The mechanism of action of surfactants on the physicochemical properties of precipitates depends on the synthetic conditions. According to the mass-spectrometric studies of thermal desorption (Fig. 4), the intensities of all peaks in the mass spectrum of a sample prepared at pH 3 are higher than the peak intensities in the spectrum of a sample prepared at pH 9 by one or two orders of magnitude. Hence, it follows that a surfactant was fixed in the sample with low pH, whereas only surfactant traces were present in the sample with high pH. This is due to the fact that, as demonstrated above, the state of components and the behavior of surfactants, in particular, EDTA, in solution depend on pH values.

The disodium salt of EDTA in solution may exist in the form of various anionic species [43], the presence of which depends on pH of the solution. Thus, at pH 2–3, carboxyl groups at which hydrogen (sodium) ions are most labile undergo dissociation [43]. At pH $\geq$ 5, hydrogen atoms are detached from the betaine nitrogen in the structure of EDTA. At pH 9 or higher, the formed complexes become unstable and undergo degradation. Consequently, at pH 3, complexes with the hydroxo complexes of both iron and zirconium can be formed. However, according to Dyatlova *et al.* [43], the interaction of an anionic EDTA species with the hydroxo complexes of iron, which are formed at the specified pH, is preferable.

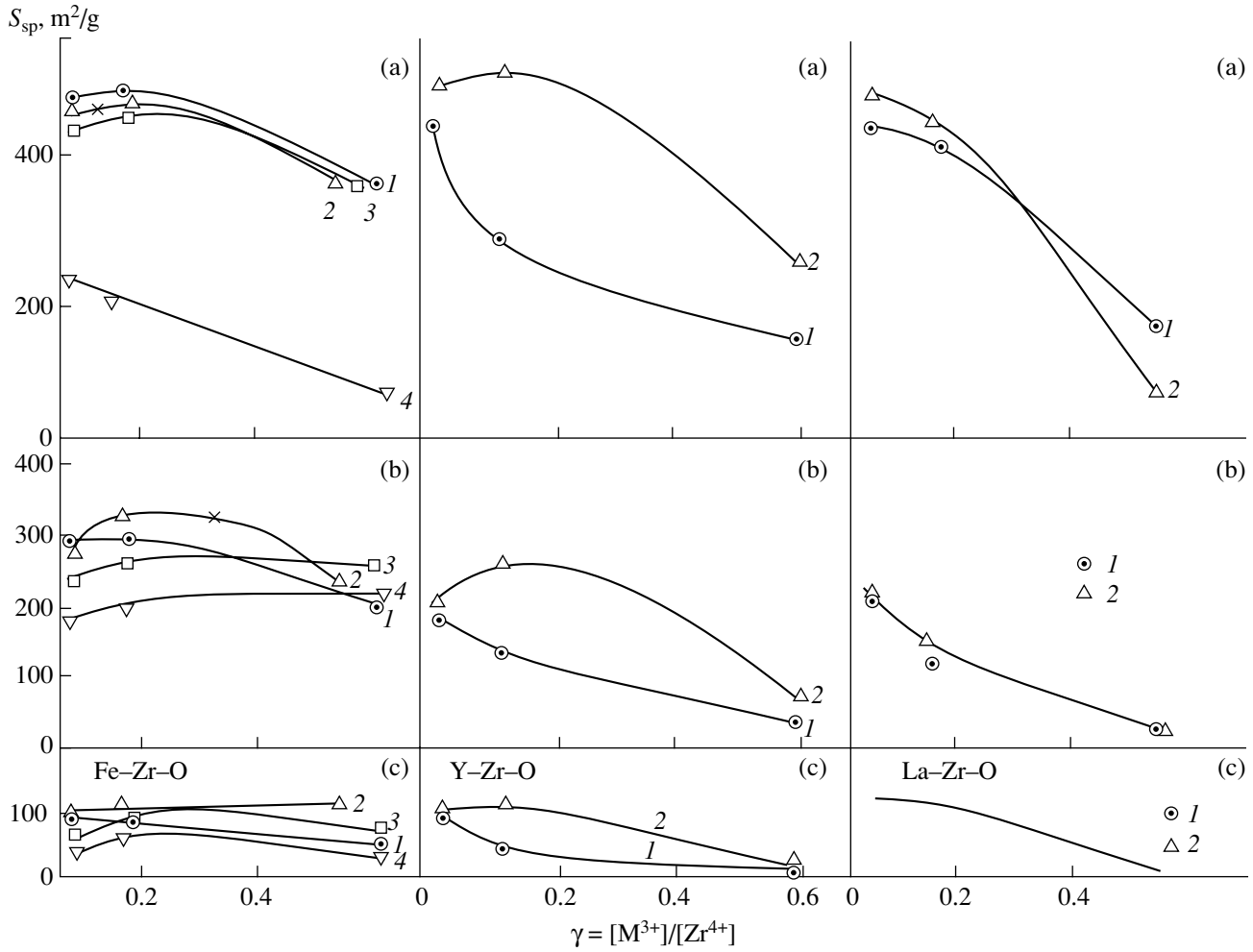

Fig. 3. Specific surface areas as functions of the ratio between components in the M–Zr–O system, where M = Fe, Y, or La, prepared at final pH (*1*, *2*) 9, (*3*) 7, and (*4*) 5 and aged for (*1*, *3*, *4*) 2 and (*2*) 5 h followed by the treatment at (a) 110, (b) 400, and (c) 700°C.

Thus, the thermolysis of samples prepared in the presence of surfactants, along with the dehydration of Fe–Zr–O compositions, is accompanied by the decomposition and degradation of surfactants. As a result of this, certain compounds and their fragments (CH_xNH_x, CH_2, CO, NO, CH_3NH_2, etc. [44]) are eliminated stepwise, and this elimination can affect the formation of the phase composition.

It can be seen in Table 1 that the phase composition of samples prepared at pH that corresponds to the complete precipitation of the components is identical regardless of the nature of surfactants, all other factors being the same. The samples calcined at 400°C are amorphous to X-rays. Only a prolongation of the aging time facilitates the formation of a highly dispersed state. The $(Zr_{1-x}Fe_x)O_{2-x/2}$ solid solution is formed after the treatment of samples in air at 700°C. The unit-cell parameter of this solid solution is 5.074–5.079 Å. This value is somewhat lower than that of pure ZrO_2; this fact indicates that Fe^{3+} enters the structure of ZrO_2.

The samples prepared at acidic pH exhibited considerable differences in the phase composition. First, at a specified ratio between components ($\gamma = 0.12$) in the presence of surfactants, samples calcined at 400°C contained α-Fe_2O_3 and a solid solution based on cubic ZrO_2 with a unit-cell parameter of 5.090–5.111 Å. This fact suggests that in the presence of surfactants the crystallization of α-Fe_2O_3 takes place. This is likely a consequence of the interaction between the hydroxo complexes of iron and EDTA at pH 3, which prevents the interaction with the hydroxo complexes of zirconium. Second, after calcination at 700°C, the samples contained magnetite (Fe_3O_4) and ZrO_2 in cubic and monoclinic modifications (Table 1). The presence of magnetite can be considered as a result of α-Fe_2O_3 reduction by compounds or their fragments released on the decomposition of surfactants.

The texture characteristics of the samples also depend on the synthetic conditions and the nature of surfactants. The addition of 1% surfactant increased the specific surface area of samples dried at 110°C and

aged at room temperature for 0.5 h by a factor of ~3–4. An increase in the temperature or in the duration of aging of the samples to 100°C or 2 h, respectively, also increased the specific surface area:

Surfactant:	0	< Glycerol	< CMC	< EDTA	< PVA
S_{sp} (T_{room}, τ_a = 0.5 h) m^2/g:	80	230	270	300	330
S_{sp} (T = 100°C, τ_a = 2 h) m^2/g:	300	480	480	500	570

In this case, the specific surface area of samples containing PVA also increased with the duration of aging; however, this increase was not so significant as that in the first hours:

τ_a, h:	2	24	48	120
S_{sp}, m^2/g:	570	605	610	650

The surface of dried samples prepared at low pH is formed in a different manner. The samples containing EDTA are coarsely dispersed (S_{sp} = 0.5 m^2/g). The replacement of EDTA with sodium stearate increased the surface area; however, it was only 110–120 m^2/g in this case. This is due to the fact that at low pH considerable amounts of low-molecular species are present along with hydroxide species [45]. Moreover, the surfactant retained by the sample up to 250–450°C (Fig. 4) blocks the porous space, and the surface of particles becomes inaccessible to adsorbate molecules.

An increase in the temperature to 400°C was accompanied by a decrease in the specific surface area to 320–400 m^2/g in the samples prepared at pH 9. In this case, differences due to the nature of surfactants almost disappeared. In the samples synthesized at pH 3, the specific surface area insignificantly increased; it is likely that this results from the removal of surfactants. A subsequent increase in the temperature to 700°C was accompanied by a decrease in the specific surface area in all samples. However, the specific surface area of

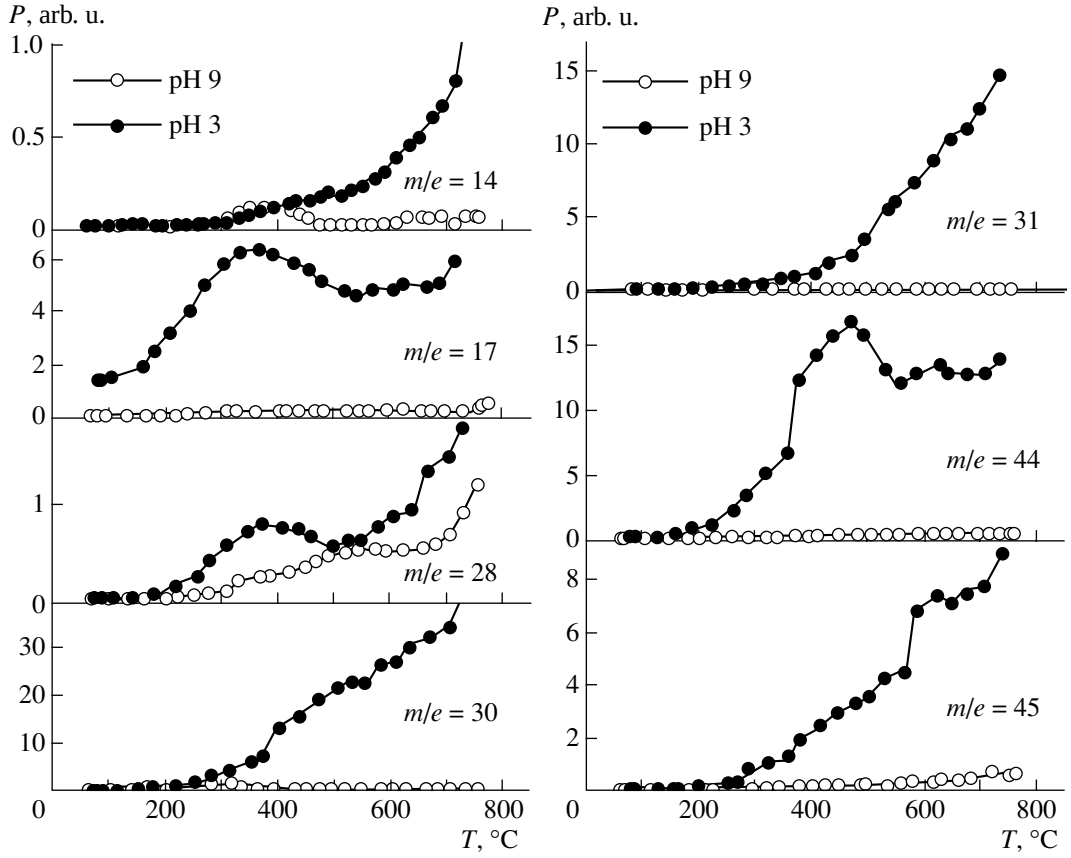

Fig. 4. Mass-spectrometric peak intensities observed on thermal desorption from Fe–Zr–O samples with EDTA added as a surfactant.

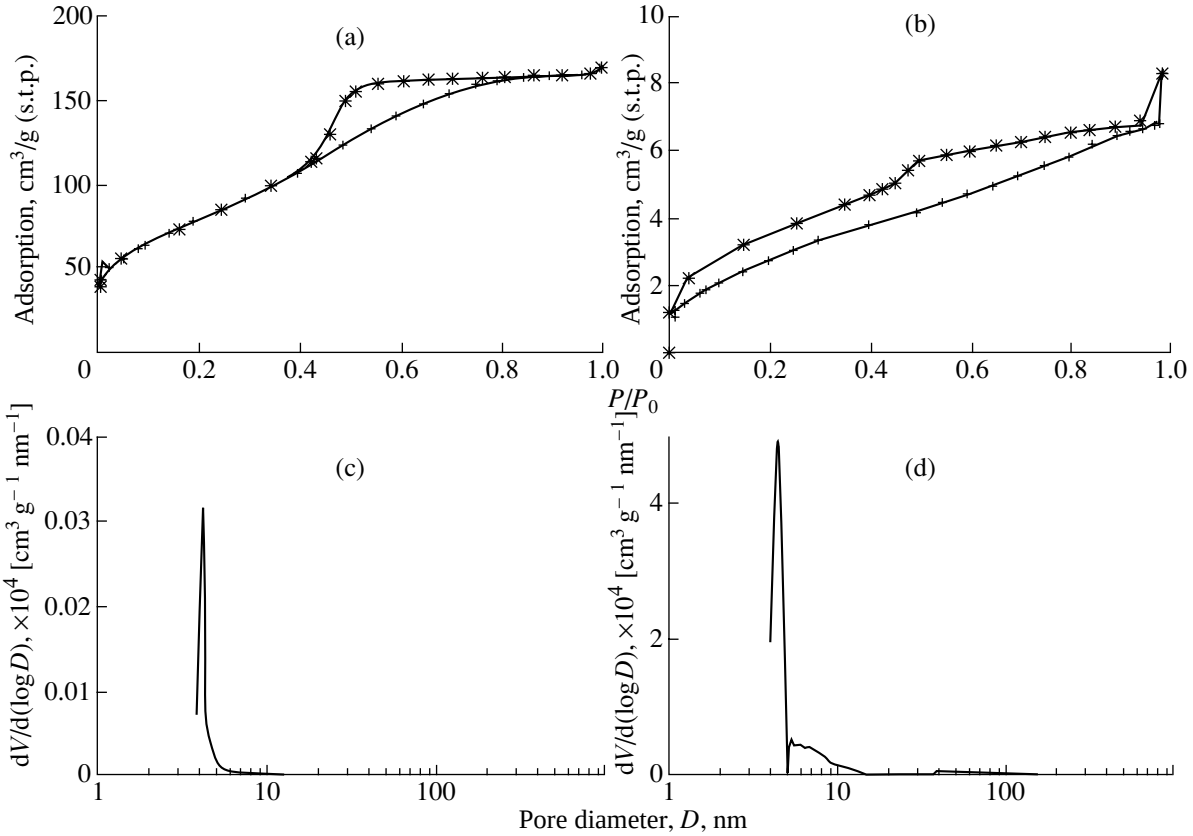

Fig. 5. (a, b) Nitrogen adsorption isotherms and (c, d) pore-size distribution for Fe–Zr–O samples prepared in the presence of EDTA at pH (a, c) 9 and (b, d) 3.

samples prepared at pH 9 or 3 was 80–100 or 5–50 m^2/g, respectively.

The isotherms of nitrogen adsorption on samples synthesized at pH 9 and calcined at 400°C exhibited identical shapes regardless of the nature of surfactants. Figure 5a demonstrates a typical adsorption isotherm, and Fig. 5b illustrates the pore-size distribution calculated from this isotherm for a sample containing EDTA. It can be seen that the sample is monomesoporous, and the average pore diameter is 3.6 nm. Changes in the

Table 1. Phase composition of iron–zirconia samples

No.	Preparation conditions			Surfactant		Phase composition; unit-cell parameter	
	pH_{final}	T, °C	τ, h	nature	amount, wt %	$T_{calcination}$, °C	
						400	700
1	9	100	2	PVA	1.0	Amorphous	$(Zr_{1-x}Fe_x)O_{2-x/2}$ (5.074, 75)
2	″	″	24	″	″	Amorphous	″
3	″	″	120	″	″	Highly dispersed state	″
4	9	100	2	EDTA	1.0	Amorphous	$(Zr_{1-x}Fe_x)O_{2-x/2}$ (5.079, 70)
5	″	″	24	″	″	Amorphous	″
6	3	100	24	″	″	α-Fe_2O_3; solid solution (5.111, 90)	Fe_3O_4; ZrO_2 (cubic) (5.112, 125) + monoclinic
7	3	100	24	Sodium stearate	5.0	α-Fe_2O_3; solid solution (5.096, 120)	Solid solution (5.102, 120)
8	3.8	″	48	″	″	α-Fe_2O_3; solid solution (5.090, 105)	″

Note: (1) Samples dried at 110°C are amorphous to X-rays. (2) The unit-cell parameter a and the coherent-scattering region in angstrom units are given in parentheses.

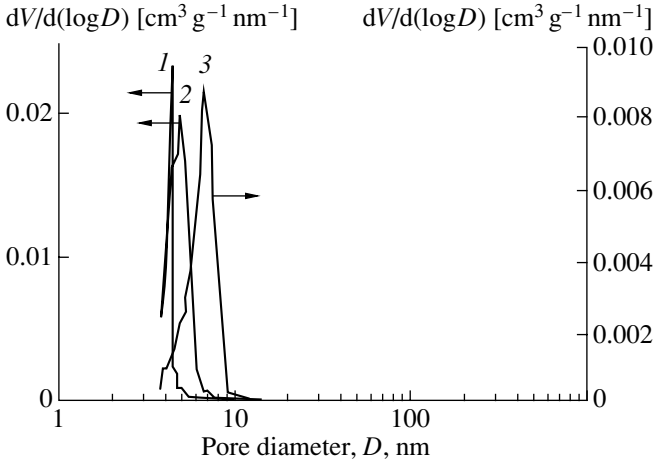

Fig. 6. Pore-size distribution in Fe–Zr–O samples prepared in the presence of PVA at pH 9: (*1*) aging for 2 h and calcination at 400°C, (*2*) aging for 120 h and calcination at 400°C, and (*3*) aging for 120 h and calcination at 700°C.

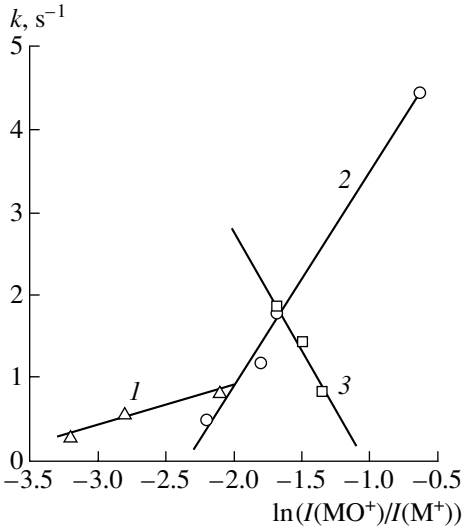

Fig. 7. Correlation between the reaction rate constant of nitrogen oxide reduction with propane in the presence of M–Zr–O catalysts and the logarithm of the ratio between ion currents $I(MO^+)/I(M^+)$ for M = (*1*) Ca, (*2*) Sr, and (*3*) Ba.

nature of surfactants and the aging time or an increase in the treatment temperature only shifted the average pore size to higher or lower values (Fig. 6).

The shape of adsorption isotherms is changed on going to the samples prepared at low pH values in the presence of EDTA (Fig. 5b): hysteresis is absent from the desorption curve, and the samples exhibit a bimodal pore-size distribution.

The total pore volume calculated from the adsorption data for samples prepared at pH 9, in particular, in the presence of PVA, increased from 0.19 to 0.35 cm^3/g with an increase in the duration of aging from 2 to 120 h. The calcination of the sample at 700°C was accompanied by a decrease in the total pore volume to 0.14 and 0.20 cm^3/g, respectively.

The total pore volume of samples prepared at pH 3 and calcined at 400°C varied within the range 0.013–0.072 cm^3/g. These values are lower than the corresponding values for the samples prepared at high pH by approximately an order of magnitude. Treatment at 700°C has almost no effect on the pore-size distribution and the total pore volume.

Thus, the synthesis of Fe–Zr–O samples by the addition of a base to salt solutions containing surfactants to a specified pH value gives highly dispersed compositions. The texture characteristics of Fe–Zr–O compositions can be controlled over wide limits by changing the preparation conditions and the nature of surfactants; either monomesoporous or bimesoporous systems can be formed.

The prepared zirconium-containing systems were found to be efficient new catalysts for the reactions given below.

The M–Zr–O systems (M = Ca, Sr, and Ba) at MO ≤ 25 mol % are active and selective catalysts for the reduction of nitrogen oxide with propane in an oxidizing atmosphere. The distinctive property of the proposed catalysts [26, 46] is that their activity increases as the reaction temperature is increased above 500°C, whereas the majority of known catalysts decreased their activity under these conditions. The rate constants of NO reduction, which were calculated by a first-order reaction rate equation, at 550°C depend on the nature and concentration of MO in M–Zr–O samples. Figure 7 demonstrates the rate constant of NO reduction as a function of the logarithm of the ratio between ion currents $I(MO^+)/I(M^+)$, which is proportional to the dissociation energy of the M–O bond in surface layers [48]. It can be seen that the rate constant linearly increases with the bond dissociation energy in Ca–Zr–O and Sr–Zr–O and decreases in Ba–Zr–O. This is likely due to the fact that the N–O bond strength in intermediate surface complexes depends on the surface state of the test samples [47–50]. In particular, Kharlanov *et al.* [50] found that the insertion of Sr into ZrO_2 impairs the electron-acceptor properties of the surface, whereas the presence of Ba enhances these properties.

The Y–Zr–O composition containing 10 mol % Y_2O_3 was an appropriate carrier for nickel catalysts for the conversion of methane by steam [28]. Note that there are many catalysts for this reaction. The proposed catalysts are designed for performing the reaction within a fuel cell. For these catalysts, oxygen conductivity provided by the $(Zr_{1-x}Y_x)O_{2-x/2}$ solid-solution carrier is one of the most important prerequisites.

It was found [28] that Ni/Y–Zr–O catalysts prepared by impregnation, mixing, and precipitation of the active component on the carrier (series I–III) are the mixtures of NiO and $(Zr_{1-x}Y_x)O_{2-x/2}$ phases, which do not interact with one another. In the synthesis of samples by the coprecipitation of components (series IV), a portion of

Table 2. Catalytic properties of M_nO_m–ZrO_2 samples in the oxidative coupling of methane

M_nO_m	M_nO_m content, mol %	S_{sp}, m^2/g	Catalytic properties**					
			$T_{reaction}$, °C	X_{CH_4}, %	S_{CO}, %	$S_{\Sigma C_2}$, %	Y_{CO}, %	$Y_{\Sigma C_2}$, %
CaO	48.6	70	700	6.8	40.4	9.7	2.8	0.7
CaO*	48.4	100	700	9.3	52.3	6.0	4.9	0.6
Sm_2O_3	52.8	20	700	2.4	41.2	13.2	1.0	0.3
Yb_2O_3	52.0	20	700	2.0	41.4	18.7	0.8	0.4

* The sample was precipitated with NH_4HCO_3.

** X is the conversion of CH_4, S is the selectivity to reaction products, and Y is the yield of products.

nickel enters $(Zr_{1-x}Y_x)O_{2-x/2}$ to result in a change in the unit-cell parameter and in an increase in the dispersion of the resulting phases. In this case, the surface area of metallic nickel in the samples of series I–III is 1.0–1.6 m^2/g Ni, whereas this value is much higher in the samples of series IV.

The above catalysts exhibit a high activity per gram of the catalyst. However, the sample activities per square meter of Ni are different for the samples of series I–III and IV. The specific activity of the samples of series I–III varies from 12 to 22 cm^3 CH_4 m^{-2} Ni s^{-1} atm^{-1}, which is consistent with the specific activity of bulk nickel catalysts [51, 52], whereas it is lower by a factor of four to five for the samples of series IV. The observed differences result from the special features of the process. According to current concepts [52], the above reaction at 700–750°C occurs via a heterogeneous–homogeneous mechanism and hence exhibits a deviation from the Boreskov rule concerning the approximate constancy of the specific activity. A similar relationship was found in [53].

The M–Zr–O compositions (M = Ca, Sm, and Yb) with approximately equimolar ratios were tested in the oxidative coupling of methane. The $MZrO_3$ systems (M = Ca, Sr, and Ba) and rare earth oxides were found [54, 55] promising for this reaction.

The acid properties of the above systems were studied previously. At different phase compositions [32], they are also characterized by nonadditive changes in the acid properties [56]. Brønsted acid sites are absent from the surface of M–Zr–O compositions calcined at 700°C; Lewis acid sites (LAS) are represented by three types of L-sites the total concentration of which decreases in the order given below.

System:	Ca–Zr–O*	< Ca–Zr–O	> Sm–Zr–O	> Yb–Zr–O
Σ[LAS]: mmol/m^2	16.0	14.1	8.4	0.5

*The sample was precipitated with NH_4HCO_3.

The main reaction products of the oxidative coupling of methane at 700–850°C are C_2 hydrocarbons, carbon oxides, hydrogen, and water [56]. The highest and lowest conversions of methane were observed on Ca–Zr–O and Yb–Zr–O samples, respectively (Table 2). However, the latter sample exhibited the highest selectivity to all ΣC_2 hydrocarbons. A maximum yield of all ΣC_2 hydrocarbons was obtained on the Ca–Zr–O sample. Table 2 demonstrates that the activity of samples (CH_4 conversion) is proportional to the specific surface area. This is likely due to the fact that the test reaction also occurs via a heterogeneous–homogeneous mechanism [57, 58], and methane is activated by the interaction with radical ionic oxygen species at the catalyst surface. The selectivity to CO is almost equal and independent of the nature of the second component, all other factors being the same. The selectivity to all ΣC_2 hydrocarbons is low, and it increases in the order Ca–Zr–O* > Ca–Zr–O > Sm–Zr–O > Yb–Zr–O; that is, a correlation between Σ[LAS] and the selectivity to all ΣC_2 hydrocarbons may be suggested.

The Ce–Zr–O system is a constituent of a catalyst for full oxidation of butane [25, 59]. Bulk M–Ce–Zr–O catalysts (M = Cr, Fe, and Co) calcined at 850°C consist of a mixture of coarsely dispersed CeO_2, cubic ZrO_2, and M_nO_m phases. Correspondingly, the activity of these catalysts in the full oxidation of butane at 400°C was ~1.2×10^{-7} mol C_4H_{10} m^{-2} s^{-1}. In M–Ce–Zr–O supported on γ-Al_2O_3 or α-Al_2O_3, the dispersion of the active component is increased, and the particle size of the formed phases is no greater than 5 nm. Chromium-containing samples were found to exhibit a maximum activity equal to 7×10^{-7} mol C_4H_{10} m^{-2} s^{-1}. Cobalt-containing samples are less active because of the formation of $CoAl_2O_4$, which is inactive in the full oxidation of hydrocarbons, at 850°C and of α-Al_2O_3, which is formed even on the deposition of an active component onto γ-Al_2O_3.

Because the active component is a complex composition, a highly active catalyst for the full oxidation of

butane was prepared by varying the order of deposition of the constituents. This catalyst exhibits enhanced thermal stability and high mechanical strength.

REFERENCES

1. Burch, R., *Zirconium in Catalysis: Its Uses and Potential*, Liverpool: University of Liverpool, 1987.
2. Rutman, D.S., Toropov, Yu.S., Plesher, S.Yu., *et al.*, *Vysokoogneupornye materialy iz dioksida tsirkoniya* (Fireproof Materials from Zirconium Dioxide), Moscow: Metallurgiya, 1985.
3. Ivanova, A.S., Dzis'ko, V.A., Ketchik, S.V., *et al.*, *Kinet. Katal.*, 1979, vol. 20, no. 3.
4. Glushkova, V.B. and Sazonova, L.V., *Khimiya vysokotemperaturnykh materialov* (Chemistry of High-Temperature Materials), Leningrad: Nauka, 1967, p. 83.
5. Nikol'skii, Yu.V., Filatov, S.K., Zhuravina, T.A., *et al.*, *Izv. Akad. Nauk SSSR, Neorg. Mater.*, 1972, vol. 8, no. 8, p. 1500.
6. Strekalovskii, V.N., Polezhaev, Yu.M., and Pal'guev, S.F., *Oksidy s primesnoi razuporyadochennost'yu* (Oxides with Admixture Disordering), Moscow: Nauka, 1987.
7. Chen, F.R., Coudurier, G., Joly, J.-F., *et al.*, *J. Catal.*, 1993, vol. 143, no. 2, p. 616.
8. Morterra, C., Cerrato, G., Pinna, F., *et al.*, *J. Phys. Chem.*, 1994, vol. 98, no. 47, p. 12373.
9. Strukul, G., Signoretto, M., Pinna, F., *et al.*, *Advanced Catalysts and Nanostructured Materials. Modern Synthetic Metholds*, Moser, W.R., Ed., New York: Academic, 1996, p. 143.
10. Yadav, G.D. and Nair, J.J., *Micropor. Mesopor. Mater.*, 1999, vol. 33, p. 1.
11. Naumov, I.I., Ol'khovik, G.A., Velikokhatnyi, O.I., *et al.*, *Neorg. Mater.*, 1992, vol. 28, no. 4, p. 805.
12. Ivanova, A.S., *Zh. Prikl. Khim.*, 1996, vol. 69, no. 11, p. 1790.
13. Ivanova, A.S., Moroz, E.M., and Litvak, G.S., *Kinet. Katal.*, 1992, vol. 33, nos. 5–6, p. 1208.
14. Viktorov, V.V. and Fotiev, A.A., *Neorg. Mater.*, 1993, vol. 29, no. 9, p. 1254.
15. *Stroenie i svoistva adsorbentov i katalizatorov* (Structure and Properties of Adsorbents), Linsen, B.G., Ed., Moscow: Mir, 1973, p. 332.
16. Baes, C.F. and Mesmer, R.E., *The Hydrolysis of Cations*, New York: Waley, 1976.
17. Povar, I.G., *Zh. Neorg. Khim.*, 1993, vol. 38, no. 11, p. 1907.
18. Il'icheva, A.A., Olenin, A.Yu., Podzorova, L.I., *et al.*, *Neorg. Mater.*, 1996, vol. 32, no. 7, p. 833.
19. Ivanova, A.S., Mikhan', M.V., Alikina, G.M., *et al.*, *Kinet. Katal.*, 2000, vol. 41, no. 6, p. 897.
20. Bastide, B., Odier, P., and Countures, J.P., *J. Am. Ceram. Soc.*, 1988, vol. 71, no. 6, p. 449.
21. Welberry, T.R., Withers, R.L., Thompson, J.G., *et al.*, *J. Solid State Chem.*, 1992, vol. 100, no. 1, p. 71.
22. Ol'khovik, G.A., Naumov, I.I., Velikokhatnyi, O.I., *et al.*, *Neorg. Mater.*, 1993, vol. 29, no. 5, p. 636.
23. Kotova, N.M., Prutchenko, S.G., and Yanovskaya, M.I., *Neorg. Mater.*, 1994, vol. 30, no. 3, p. 387.
24. Ivanova, A.S., Alikina, G.M., Solov'eva, L.P., *et al.*, *Tezisy dokladov IV Evropeiskoi konferentsii po materialam i tekhnologiyam* (Proc. IV Eur. Conf. on Materials and Technologies), St. Petersburg, 1993, vol. 1, p. 23, (A-8R).
25. Ivanova, A.S. and Moroz, E.M., *Kinet. Katal.*, 1995, vol. 36, no. 1, p. 127.
26. Ivanova, A.S., Alikina, G.M., Solovyova, L.P., *et al.*, *React. Kinet. Catal. Lett.*, 1996, vol. 59, no. 1, p. 125.
27. Ivanova, A.S., Moroz, E.M., and Ivanov, V.P., *Tezisy dokladov Vserossiiskoi konferentsii "Khimiya tverdogo tela i novye materially"* (Proc. All-Russsia Conf. on Solid-State Chemistry and New MAterials), Ekaterinburg, 1996, vol. 2, p. 47.
28. Ivanova, A.S., Bobrova, I.I., Moroz, E.M., *et al.*, *Kinet. Katal.*, 1997, vol. 38, no. 1, p. 114.
29. Polezhaev, Yu.M., Barbina, T.M., and Polezhaev, V.Yu., *Neorg. Mater.*, 1994, vol. 30, no. 7, p. 959.
30. Zaitseva, I.A. and Dobrokhotova, Zh.V., *Neorg. Mater.*, 1994, vol. 30, no. 7, p. 955.
31. Leonov, A.I., *Vysokotemperaturnaya khimiya kislorodnykh soedinenii tseriya* (High-Temperature Chemistry of Oxygen-Containing Cerium Compounds), Leningrad: Nauka, 1970, p. 123.
32. Ivanova, A.S., Moroz, E.M., and Litvak, G.S., *React. Kinet. Catal. Lett.*, 1998, vol. 65, no. 1, p. 169.
33. Fedotov, M.A., Krivoruchko, O.P., Golovin, A.V., *et al.*, *Izv. Akad. Nauk SSSR, Ser. Khim.*, 1977, no. 2, p. 473.
34. Krivoruchko, O.P., Buyanov, R.A., Fedorov, M.A., *et al.*, *Zh. Neorg. Khim.*, 1978, vol. 27, no. 7, p. 1798.
35. Fedotov, M.A., Taraban, E.A., and Buyanov, R.A., *Zh. Neorg. Khim.*, 1993, vol. 38, no. 11, p. 1849.
36. Ivanova, A.S., Fedotov, M.A., Litvak, G.S., *et al.*, *Neorg. Mater.*, 2000, vol. 36, no. 4, p. 440.
37. Lukachina, E.N., Stetsenko, V.I., and Ermolenko, I.V., *Izv. Akad. Nauk SSSR, Neorg. Mater.*, 1978, vol. 14, no. 1, p. 102.
38. *Khimiya redkikh i rasseyannykh elementov* (Chemistry of Rare and Scattered Elements), Bol'shakov, K.A., Ed., Moscow: Vysshaya Shkola, 1965, vol. 1, p. 138.
39. Zyuzin, D.A., Moroz, E.M., Ivanova, A.S., *et al.*, *Neorg. Mater.*, 2000, vol. 36, no. 4, p. 447.
40. Moroz, E.M., Ivanova, A.S., and Ziouzin, D.A., *Abstr. Memorial K.I. Zamaraev Conf. "Physical Methods for Catalytic Research at the Molecular Level," Novosibirsk*, 1999, p. 117 (PPI-30).
41. Dzis'ko, V.A., Karnaukhov, A.P., and Tarasova, D.V., *Fiziko-khimicheskie osnovy sinteza oksidnykh katalizatorov* (Physicochemical Fundamentals for the Synthesis of Oxide Catalysts), Novosibirsk: Nauka, 1978.
42. Ivanova, A.S., Fedotov, M.A., Litvak, G.S., *et al.*, *Kinet. Katal.*, (in press).
43. Dyatlova, N.M., Temkina, V.Ya., and Kolpakova, I.D., *Kompleksony* (Comlexons), Moscow: Khimiya, 1970, p. 23.
44. Sidel'nikov, V.N., Gur'yanova, L.V., Utkin, V.A., *et al.*, *Katalog sokrashchennykh mass-spektrov* (Catalog of Contracted Mass Spectra), Kolchin, A.M., Ed., Novosibirsk: Nauka, 1981.
45. Gavrilov, V.Yu. and Zenkovets, G.A., *Kinet. Katal.*, 2000, vol. 41, no. 4, p. 617.

46. RF Patent 2043146, 1995.
47. Sadykov, V.A., Baron, S.L., Matyshak, V.A., *et al.*, *Catal. Lett.*, 1996, vol. 37, nos. 3–4, p. 157.
48. Wittmaack, K., *Surf. Sci.*, 1979, vol. 89, nos. 3–4, p. 668.
49. Sadykov, V.A., Ivanova, A.S., Alikina, G.M., *et al.*, *Mater. Research Society (Symposium Proceeding Series)*, 1997, vol. 454, p. 199.
50. Kharlanov, A.N., Zubareva, N.A., Lunina, E.V., *et al.*, *Vestn. Mosk. Univ., Ser. 2: Khim.*, 1998, vol. 39, no. 1, p. 29.
51. Bodrov, I.M., Appel'baum, L.O., and Temkin, M.I., *Kinet. Katal.*, 1964, vol. 5, no. 4, p. 696.
52. Bobrov, N.N., Bobrova, I.I., and Sobyanin, V.A., *Kinet. Katal.*, 1993, vol. 34, no. 4, p. 686.
53. Golodets, G.I. and Il'chenko, N.I., *Kinet. Katal.*, 1995, vol. 36, no. 1, p. 33.
54. Matsuda, N., Ohyachi, K., and Matsuura, I., *Chem. Express*, 1990, vol. 5, p. 533.
55. Choudhary, V.R. and Rane, V.H., *J. Catal.*, 1991, vol. 130, p. 411.
56. Ivanova, A.S., Paukshtis, E.A., Sobyanin, V.A., *et al.*, *React. Kinet. Catal. Lett.*, 1998, vol. 64, no. 2, p. 337.
57. Krylov, O.V., *Usp. Khim.*, 1992, vol. 61, no. 8, p. 1550.
58. Chernyshkova, F.A., *Zh. Prikl. Khim.*, 1994, vol. 67, no. 4, p. 542.
59. USSR Inventor's Certificate no. 1641416, *Byull. Izobret.*, 1991, no. 14.